

Nonlinear vibration and adhesion instability of Casimir-induced nonlocal nanowires with the consideration of surface energy

Hamid M. Sedighi¹ · Alireza Bozorgmehri²

Received: 28 October 2015 / Accepted: 16 March 2016 / Published online: 30 March 2016
© The Brazilian Society of Mechanical Sciences and Engineering 2016

Abstract The following research work deals with the size-dependent dynamic instability of suspended nanowires in the presence of Casimir force and surface effects. Specifically, the Casimir-induced instability of nanostructures with circular cross-section and cylinder-plate geometry is studied. Following the Gurtin–Murdoch model and nonlocal elasticity, the governing equation of motion for nanowires is derived. To express the Casimir attraction of cylinder-plate geometry, two approaches, e.g. proximity force approximation (PFA) for small separations and Dirichlet asymptotic approximation for large separations are studied. To overcome the difficulties for solving a nonlinear problem, a step-by-step numerical method is utilized. The effects of nonlocal parameter, surface energy and vacuum fluctuations on the dynamic instability characteristic and adhesion time of nanowires are studied. It is observed that the phase portrait of Casimir-induced nanowires exhibit periodic and homoclinic orbits.

Keywords Suspended cylindrical nanowire · Casimir force · Proximity force approximation (PFA) · Dirichlet asymptotic approximation

Technical Editor: Kátia Lucchesi Cavalca Dedini.

✉ Hamid M. Sedighi
hmsedighi@gmail.com; h.msedighi@scu.ac.ir
Alireza Bozorgmehri
a.r.bozorgmehri@gmail.com

¹ Mechanical Engineering Department, Faculty of Engineering, Shahid Chamran University of Ahvaz, Ahvaz, Iran

² Mechanical Engineering Department, Faculty of Engineering, Shohadaye Hoveizeh University of Technology, Dasht-e-Azadegan, Iran

1 Introduction

Because of excellent physical properties of nanowire-based nano-structures, e.g. small size with large ratio of surface-area to volume, the applications of these structures are growing rapidly. Nanowires are of great interest for detecting nano-objects with high sensitivity and also have noticeable applications in several industries such as optics [1], nanoelectromechanical systems (NEMS) [2], biological or gas sensing devices [3], flexible electronics and renewable energy technologies [4], ultrasensitive biological and chemical sensors [5], pH measurements [6], resonators and actuators [7, 8] and multifunctional NEMS.

When the electronic and mechanical systems are fabricated at nano-scale size, some new phenomena that originated from the nano-size quantum effects have become more important and the motion of nanowire-based structure is affected by the small-scale quantum electrodynamic interactions such as vacuum fluctuations. The effect of vacuum fluctuation forces is usually modeled through the Casimir attraction which is the dominant phenomenon in sub-micron separations [9]. By integrating a force-sensing micromechanical beam and an electrostatic actuator on a single chip, Zou et al. [10] demonstrated the Casimir effect between two micromachined silicon components on the same substrate. Lombardo et al. [11] numerically evaluate the Casimir interaction energy for configurations involving two perfectly conducting eccentric cylinders and a cylinder in front of a plane. Emig et al. [12] found the exact Casimir force between a plate and a cylinder by assuming an intermediate geometry between parallel plates and the plate-sphere. Tercas et al. [13] considered the mechanical coupling between a two-dimensional Bose–Einstein condensate and a graphene sheet via the vacuum fluctuations

of the electromagnetic field which are at the origin of the so-called Casimir–Polder potential. By deriving a self-consistent set of governing equations of the condensate and the flexural modes of the graphene, they could show the formation of a new type of purely acoustic quasi-particle excitation, a quasi-polariton resulting from the coherent superposition of quanta of flexural and Bogoliubov modes. Ali et al. [14] investigated the excitation of electrostatic wake fields in metallic nanowires due to the propagation of a short electron pulse. To this end, they considered a non-local dielectric response of the system and discussed the stability conditions of wake fields. Moreover, they showed that the underlying mechanism can be useful to investigate new sources of radiation in the extreme-ultraviolet range. Bordag et al. [15] provided a review of both new experimental and theoretical developments in the Casimir effect. They demonstrated that the Casimir force strongly depends on the shape, size, geometry and topology of the boundaries. Since then, many investigations have been conducted to compute the Casimir attraction for different geometries including parallel plates [16–18], plate-sphere [19], parallel cylinders [20] and plate-cylinder [21]. Several investigations have investigated the instability characteristics and nonlinear analysis of micro/nano-scale structures by employing different assumptions and theories such as nonlocal elasticity [22–24] modified couple stress theory [25–28], strain gradient theory [29, 30], modified strain gradient theory [31], strain-inertia gradient elasticity [32], etc. A nano-scale device might adhere to its substrate due to Casimir force if the minimum gap between the flexible beam and the substrate is not considered. Besides interfering with the stability of freestanding nanostructures, the Casimir force can also induce undesired adhesion during the fabrication stages. Therefore, the investigation on the stability behavior of suspended nanowires is very crucial for precise designing and mounting of these structures. All the published works have focused on the instability analysis of small-sized structures with planar or rectangular cross-section. However, the dynamic instability characteristics of size-dependent nano-beams with circular cross-section with the consideration of Casimir force by incorporating the surface effects have not been addressed so far.

Owing to the high surface/volume ratio of nano-sized structures [33], it was experimentally demonstrated that the surface layer plays an important role in the static and dynamic behavior of such devices. Atoms at a free surface of nano-structures experience a different local environment with respect to the atoms in the bulk material. Consequently, the energy associated with these atoms is different from that of the atoms in the bulk. The excess energy associated with surface atoms is called surface free energy [34]. In the classical continuum mechanics, the effect of surface layer is ignored. However, for nano-size devices, due to the

high surface-to-volume ratios, the influence of the surface layer on the overall dynamic behavior of nano-structure becomes highlighted. A surface elasticity theory was presented by Gurtin and Murdoch [35] to model the surface layer of a solid as a membrane with negligible thickness. The dynamic pull-in behavior of an electrically actuated nano-bridge with rectangular cross-section incorporating the surface and small-size effects was studied by Sedighi [36]. Eltahir et al. [37] examined the vibration characteristics of nano-beams using the nonlocal finite element model with the consideration of surface layer effects. The pull-in behavior of an electrically actuated nano-beam by incorporating surface elasticity was studied by Fu and Zhang [38]. They solved the complex mathematical problem by the analog equation method (AEM) and discussed the effects of the surface energies on the static and dynamic responses, pull-in voltage and pull-in time. The influence of surface effect on the static instability behavior of cantilever nano-actuator in the presence of van der Waals force (vdW) was investigated by Koochi et al. [39].

As mentioned earlier, the Casimir force can induce instability and adhesion in suspended nanostructures. Based on the available published literature, previous investigations in this area have focused on modeling instability in structures with planar or rectangular cross-section and the Casimir-induced instability and dynamic behavior of nano-systems with circular cross-section (such as nanowires and nanotubes) have not been explored yet. Therefore, the main objective of this study was to examine the influence of Casimir attraction on the instability/adhesion characteristics of nano-bridges incorporating the size-dependency and surface layer effects. To this end, the nonlocal elasticity together with the Euler–Bernoulli beam theory is adopted to derive the vibrational governing equation of nanowires with the consideration of vacuum fluctuations and surface energy. To solve the nonlinear governing equation a stepwise numerical method is introduced. Finally, the effect of different parameters on the instability behavior and adhesion time of Casimir-induced suspended nanowires is addressed.

2 Mathematical modeling

The schematic view and SEM image of suspended doubly clamped nanowire above a flat plate substrate is depicted in Fig. 1. The flexible cylinder can deform towards the fixed ground plane due to the influence of Casimir attractive force. The nanowire has the initial gap D , length L and radius R . In the following subsections, based on two different approaches, e.g. PFA (small separation approximation) and Dirichlet mode (large separation approximation), the governing equation of Casimir-induced nanowires are extracted.

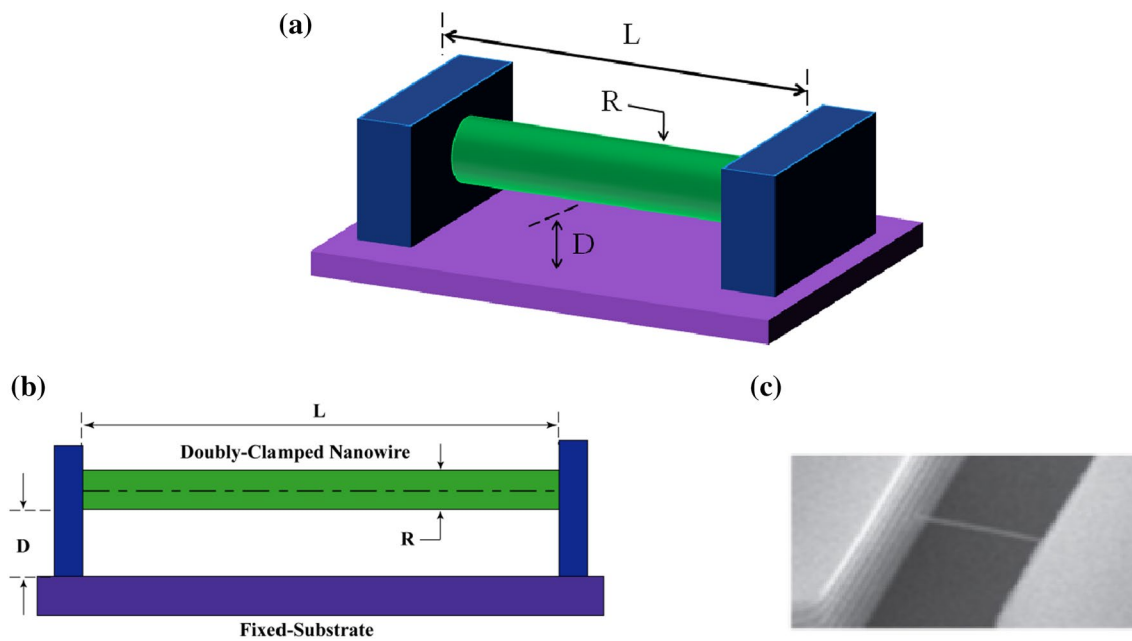


Fig. 1 a Schematics view b side view and c SEM image of doubly clamped cylinder-plate

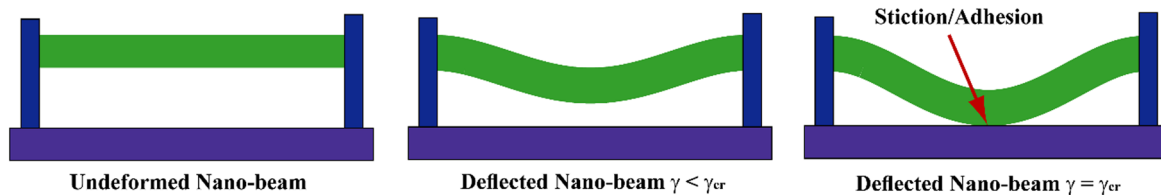


Fig. 2 Adhesion phenomena of suspended doubly clamped nanowire under Casimir attraction

Figure 2 shows the schematic representation of a doubly clamped nanowire suspended on three substrates. When the interface force that originates from Casimir attraction between two surfaces is smaller than the critical value, the nanowire deflected toward the fixed substrate. As the Casimir force increases and approaches the critical value, the nanowire cannot tolerate the attractive load and suddenly collapses on the lower plate and the stiction/adhesion phenomena occurs [40].

2.1 Equation of motion

The configuration of a doubly clamped nanowire with consideration of surface layer is shown in Fig. 3a. Based on the Gurtin–Murdoch method [35], it is assumed that the nanowire has an elastic surface with zero thickness with specific material characteristics which accounts for the surface energy effects. Moreover, Fig. 3b shows the free-body diagram of an infinitely small nano-beam element. The governing equation for transverse vibration of nanowire is expressed as follows [38]:

$$\frac{\partial^2 M}{\partial x^2} - \frac{\partial}{\partial x} \int_S T_z ds - q(x, t) - \frac{\partial}{\partial x} \left(N \frac{\partial w}{\partial x} \right) + (\rho A)_{\text{eff}} \frac{\partial^2 w}{\partial t^2} = 0, \tag{1}$$

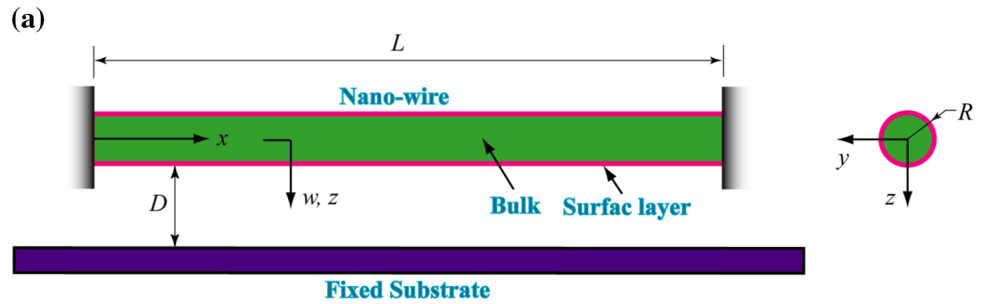
where T_x and T_z refer to the contact tractions between the surface layer and bulk material, respectively. M is the bending moment, N is the axial force, S is the perimeter of the cross-section and $q(x, t)$, that is derived in the subsequent section, denotes the Casimir force per unit length of the nanowire.

The relation between the contact traction and the surface layer stresses is written as

$$\frac{\partial \tau_{ix}}{\partial x} - T_i = \rho_0 \frac{\partial^2 u_i^s}{\partial t^2}, \tag{2}$$

where $i = x, z$, ρ_0 represents the mass density of surface layer and u_i^s is the deflection of the surface layer in the i direction. The constitutive equations for the surface layer and the governing equations for the axial force and bending moment are given by

Fig. 3 **a** Schematic representation of a doubly clamped nanowire and **b** nano-beam element



$$N = \frac{EA}{2L} \int_0^L \left(\frac{\partial w}{\partial x} \right)^2 dx + N_0 \tag{3}$$

$$M = (EI)_{\text{eff}} \frac{\partial^2 w}{\partial x^2} - \frac{2\nu I}{2R} \left(\tau_0 \frac{\partial^2 w}{\partial x^2} - \rho_0 \frac{\partial^2 w}{\partial t^2} \right) \tag{4}$$

$$\tau_{xx} = \tau_0 + E_0 \left(\frac{\partial u}{\partial x} - z \frac{\partial^2 w}{\partial x^2} \right) \tag{5}$$

$$\tau_{zx} = \tau_0 \frac{\partial w}{\partial x} \tag{6}$$

Substituting of Eq. (2) into Eq. (1) and using the above-mentioned relations results in

$$\begin{aligned} & \left[EI + E_0 I_0 - \frac{2\nu I \tau_0}{2R} \right] \frac{\partial^4 w}{\partial x^4} + [\rho A + \rho_0 S_0] \frac{\partial^2 w}{\partial t^2} + \frac{\nu I \rho_0}{R} \frac{\partial^4 w}{\partial x^2 \partial t^2} \\ & = q(x, t) + \left[\tau_0 S_0 + \frac{EA}{2L} \int_0^L \left(\frac{\partial w}{\partial x} \right)^2 dx + N_0 \right] \frac{\partial^2 w}{\partial x^2}, \end{aligned} \tag{7}$$

where E_0 is the elasticity of surface layer, $I_0 = \int_S z^2 ds$ represents the perimeter moment of inertia, τ_0 is the initial residual surface stress and ν is the Poisson's ratio of the

bulk material. The nonlocal constitutive equations for the nanowire are given by

$$(1 - e_0^2 a^2 \Delta^2) M^{\text{nl}} = M^l \tag{8}$$

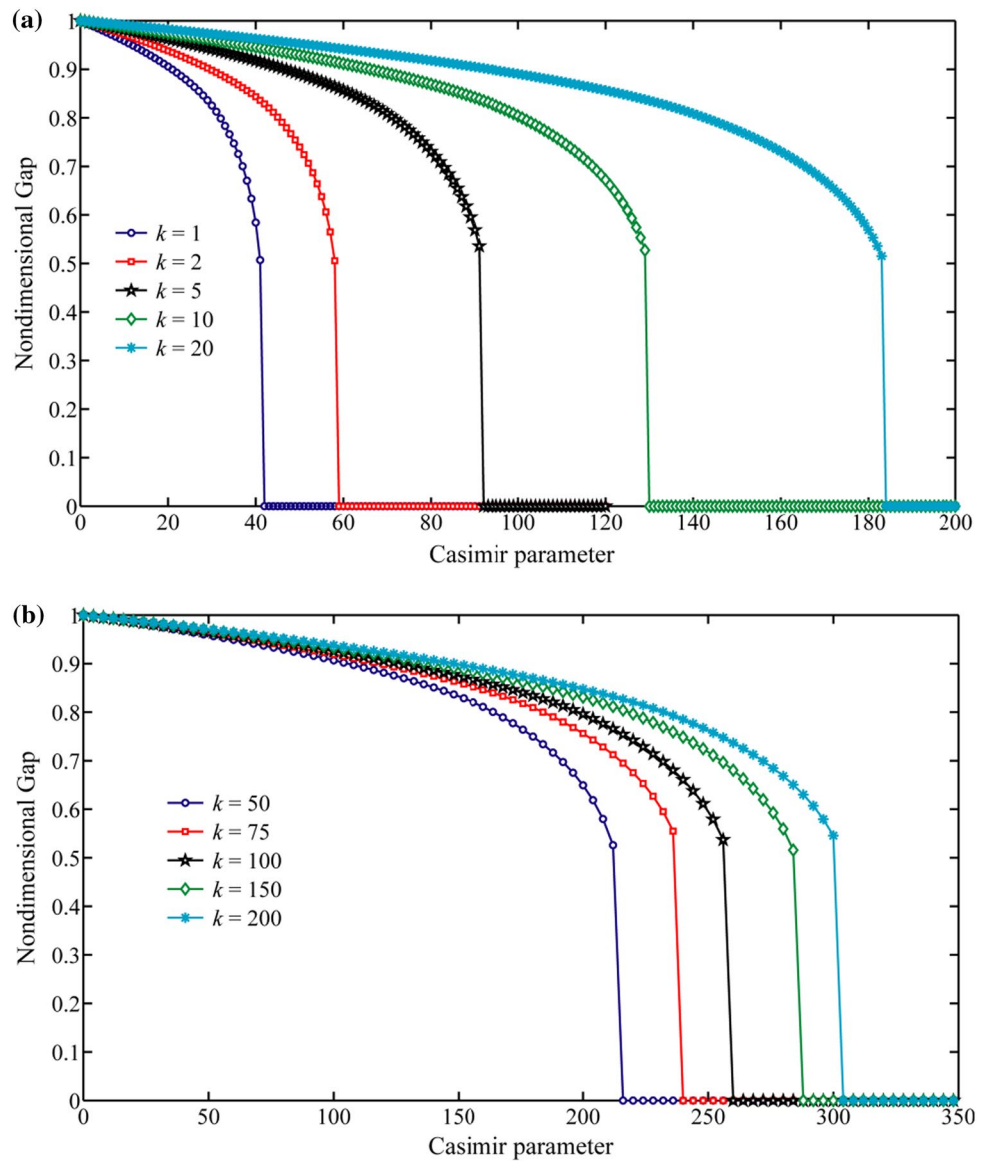
$$(1 - e_0^2 a^2 \Delta^2) \tau_{xx}^{\text{nl}} = \tau_{xx}^l \tag{9}$$

$$(1 - e_0^2 a^2 \Delta^2) \tau_{zx}^{\text{nl}} = \tau_{zx}^l, \tag{10}$$

where $\Delta^2 = \partial^2 / \partial x^2$, e_0 and a represent the nonlocal effects dependent on material and an internal characteristic length nanoscale. Rewriting the governing equation described in Eq. (1) in the nonlocal form and multiplied by the nonlocal operator $(1 - e_0^2 a^2 \Delta^2)$, the governing equation for the Casimir-induced nonlocal nanowires is obtained as

$$\begin{aligned} & \left[EI + E_0 I_0 - \frac{2\nu I \tau_0}{2R} \right] \frac{\partial^4 w}{\partial x^4} + \frac{\nu I \rho_0}{R} \frac{\partial^4 w}{\partial x^2 \partial t^2} - \tau_0 S_0 \frac{\partial^2 w}{\partial x^2} = \\ & (1 - e_0^2 a^2 \Delta^2) \left[q(x, t) + \left(N_0 + \frac{EA}{2L} \int_0^L \left(\frac{\partial w}{\partial x} \right)^2 dx \right) \frac{\partial^2 w}{\partial x^2} \right. \\ & \left. - (\rho A + \rho_0 S_0) \frac{\partial^2 w}{\partial t^2} \right] \end{aligned} \tag{11}$$

Fig. 4 Non-dimensional gap versus the Casimir parameter: investigating the effect of geometry parameter k for **a** SSA **b** LSA approaches



Equation (11) is subjected to the boundary conditions as follows:

$$w(0, t) = 0, w'(0, t) = 0, w(L, t) = 0, w'(L, t) = 0, \quad (12)$$

In addition, the initial conditions of nano-structure are defined as

$$w(x, 0) = 0, \dot{w}(x, 0) = 0, \quad (13)$$

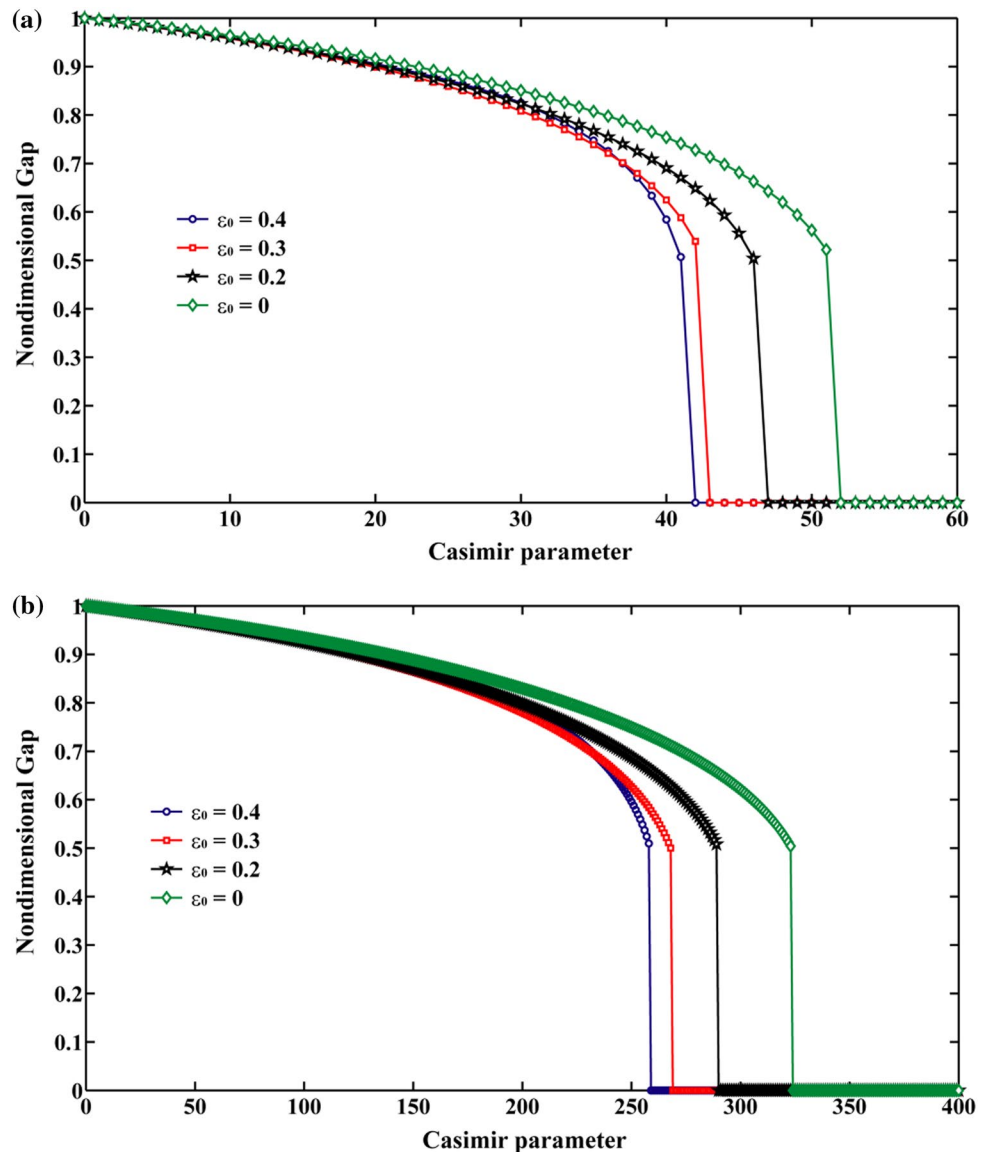
2.2 Casimir force for the cylinder-plate geometry

For the case of conducting parallel flat plates, the Casimir energy per unit area separated by a distance D is [41]

$$E_{pp}(D) = -\frac{\pi^2 \bar{h} c}{720 D^3}, \quad (14)$$

where c is the light speed and \bar{h} is Planck’s constant. It should be noted that this formula can be obtained with the consideration of the electromagnetic mode structure between the two plates in comparison with the free space by assigning a zero-point energy to each electromagnetic mode [42]. Proximity force approximation (PFA) fundamentally uses the relation described in Eq. (14) to predict the Casimir force in the case of small separation. Based on PFA approach, the interaction between any other surfaces

Fig. 5 Non-dimensional gap versus the Casimir parameter: investigating the effect of nonlocal parameter ϵ_0 for **a** SSA **b** LSA approaches



is modeled through a summation of infinitesimal parallel plates [41]. For small separations, the correct zeroth order approximation for the Casimir energy is given by [10]

$$E^{\text{PFA}} = \int_S E_{\text{PP}}(D) dS = -\frac{\pi^2 \hbar c}{720} \iint \frac{dS}{D^3}, \tag{15}$$

in which S is one of the two surfaces restricting a gap. It should be emphasized that for large separation as well as non-smooth surfaces the PFA cannot be used. Therefore, another approach should be employed to model the Casimir attraction force for the case of larger separations. To model the Casimir energy in large separations, a path integral representation [43] is used and the electrodynamic Casimir energy of two disconnected metallic surfaces using Dirichlet mode definition at zero temperature is determined

[44, 45]. The Casimir energy of this mode at zero temperature is expressed as

$$E^D = \frac{\hbar c}{2\pi} \int_0^\infty \text{Tr} \ln(MM_\infty^{-1}) dq_0, \tag{16-a}$$

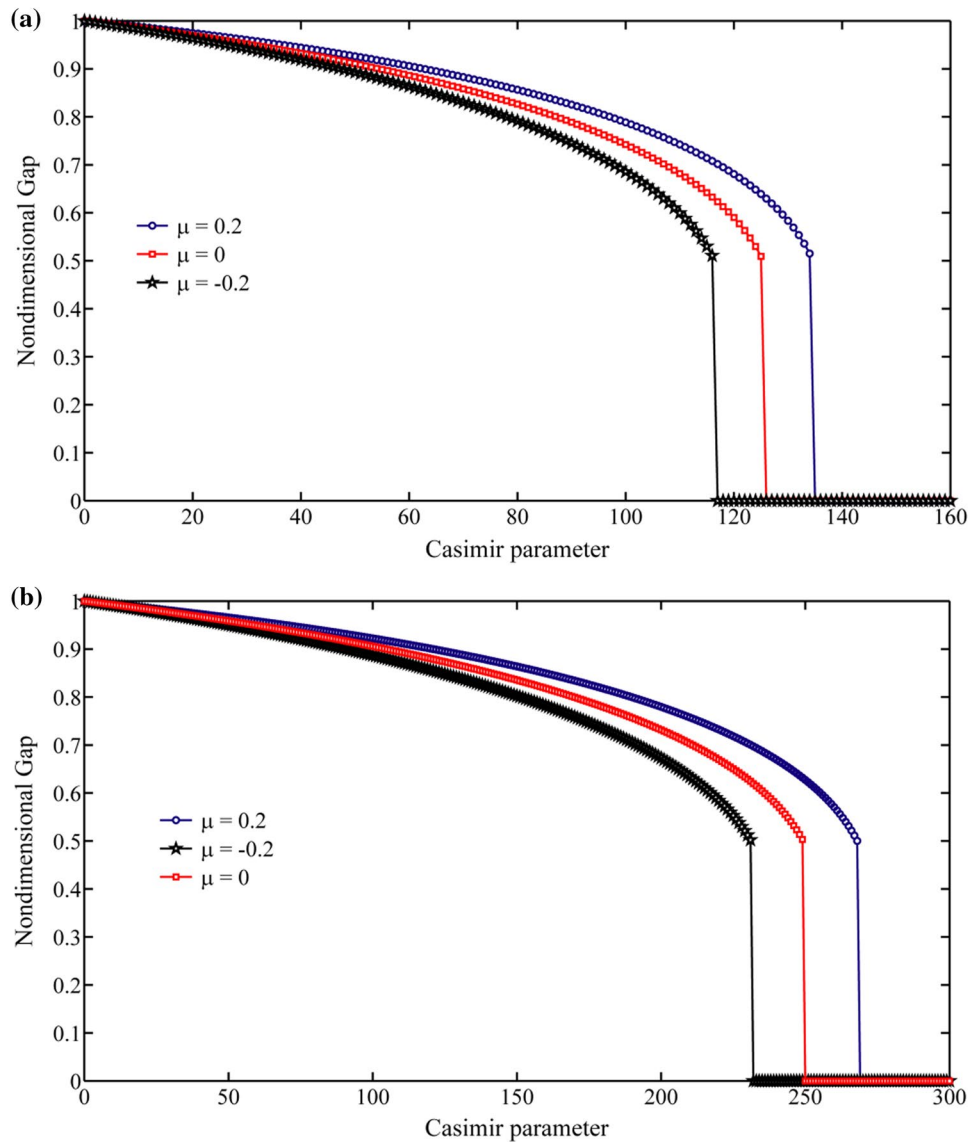
in which

$$M_{12}(u, u'; q_0) = G_0(s_1(u) - s_2(u'); q_0), \tag{16-b}$$

$$G_0(x, x'; q_0) = \frac{e^{-q_0|x-x'|}}{4\pi|x-x'|},$$

where matrix M_{12} represents the geometry of the surfaces 1 and 2, M_∞^{-1} is the functional inverse of matrix M at infinite surface separation, $s_i(u)$ is a vector referring to

Fig. 6 Non-dimensional gap versus the Casimir parameter: investigating the effect of surface effect parameter μ for **a** SSA **b** LSA approaches



the i th surface parameterized by the surface vector u and G_0 denotes the free space Green function [46]. Based on the PFA (for small separations), the Casimir energy can be obtained as [10]

$$E^{\text{PFA}} = -\frac{\pi^3 \hbar c L}{960} \sqrt{\frac{R}{2D^5}}, \tag{17}$$

where R denotes the radius of nanowire and D is the gap distance. Thus, the Casimir force for small separation approximation (SSA) can be obtained by differentiating the energy with respect to D as

$$f_{\text{cas}} = -\frac{\partial E(D)}{\partial D} = \frac{1}{768} \pi^3 \hbar c L \sqrt{\frac{2R}{D^7}} \tag{18}$$

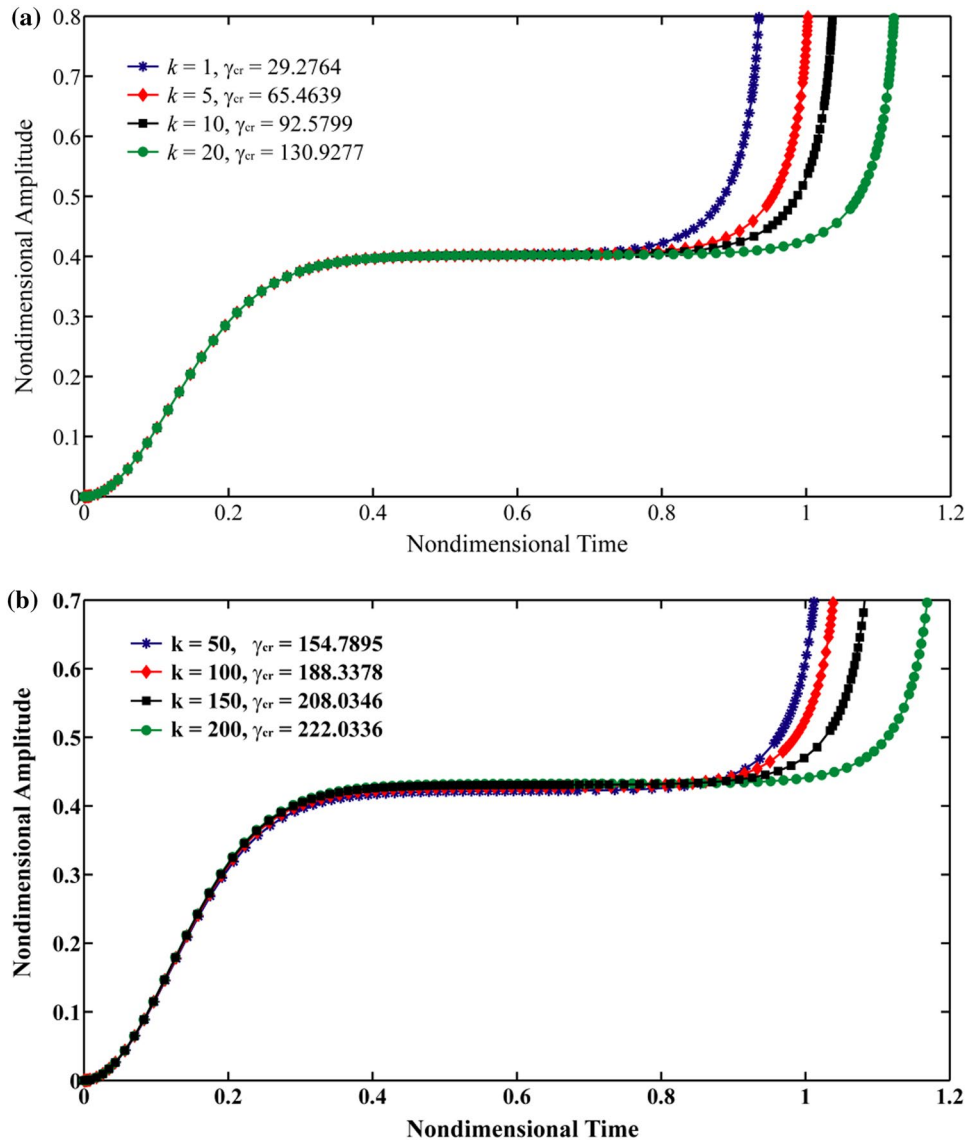
Otherwise, for the case of cylinder-plate geometry with large separation gap, i.e. $D \gg R$, the approximate expression for the attractive Casimir energy is stated as [47]

$$E^D = -\frac{\hbar c L}{D^2} \frac{1}{16\pi \ln(\frac{D}{R})}; \tag{19}$$

therefore, the Casimir force for large separation approximation (LSA) can be expressed as follows:

$$f_{\text{cas}} = \frac{\hbar c L}{D^3} \frac{1}{8\pi \ln(\frac{D}{R})} + \frac{\hbar c L}{D^3} \frac{1}{16\pi \ln^2(\frac{D}{R})} \tag{20}$$

Fig. 7 Time responses of nanowires at corresponding instability state: investigating the effect of geometry parameter k for **a** SSA **b** LSA approaches



2.3 Nondimensionalization of governing equation

In order to express the governing equation in the non-dimensional form, the following variables are defined:

$$\begin{aligned} \tau &= \sqrt{\frac{EI}{\rho b h L^4}} t, \quad W = \frac{w}{D}, \quad \xi = \frac{x}{L}, \quad \alpha = \frac{EAD^2}{2EI}, \quad k = \frac{D}{R}, \quad \mu = \frac{E_0 I_0}{EI}, \\ \sigma_1 &= \frac{\nu \tau_0}{ER}, \quad \sigma_2 = \frac{\tau_0 S_0 L^2}{EI}, \quad \gamma = \frac{\bar{h} c L^4}{8\pi D^4 EI}, \quad f_i = \frac{N_0 L^2}{EI}, \quad \varepsilon_0 = \frac{e_0 a}{L}, \\ \kappa_1 &= \frac{\nu \rho_0 R}{3\rho L^2}, \quad \kappa_2 = \frac{\rho_0 S_0}{\rho A} \end{aligned} \tag{21}$$

Thereby, the non-dimensional equation of motion for nonlocal nanowires considering the surface effects and Casimir force can be written as

$$\begin{aligned} &(1 + \mu - \sigma_1) \frac{\partial^4 W}{\partial \xi^4} + \kappa_1 \frac{\partial^4 W}{\partial \xi^2 \partial \bar{\tau}^2} - \sigma_2 \frac{\partial^2 W}{\partial \xi^2} \\ &= \left(1 - \varepsilon_0^2 \frac{\partial^2}{\partial \xi^2}\right) \left[\frac{\pi^4 \gamma}{96} \sqrt{\frac{2}{k(1-W)^7}} \right. \\ &\quad \left. + \left(f_i + \alpha \int_0^1 \left(\frac{\partial W}{\partial \xi}\right)^2 d\xi \right) \frac{\partial^2 W}{\partial \xi^2} - (1 + \kappa_2) \frac{\partial^2 W}{\partial \bar{\tau}^2} \right] \end{aligned} \tag{22-a}$$

for SSA approximation and

$$\begin{aligned} &(1 + \mu - \sigma_1) \frac{\partial^4 W}{\partial \xi^4} + \kappa_1 \frac{\partial^4 W}{\partial \xi^2 \partial \bar{\tau}^2} - \sigma_2 \frac{\partial^2 W}{\partial \xi^2} \\ &= \left(1 - \varepsilon_0^2 \frac{\partial^2}{\partial \xi^2}\right) \left[\frac{\gamma}{(1-W)^3} \frac{1}{\ln(k(1-W))} + \frac{\gamma}{(1-W)^3} \frac{1}{2(\ln(k(1-W)))^2} \right. \\ &\quad \left. + \left(f_i + \alpha \int_0^1 \left(\frac{\partial W}{\partial \xi}\right)^2 d\xi \right) \frac{\partial^2 W}{\partial \xi^2} - (1 + \kappa_2) \frac{\partial^2 W}{\partial \bar{\tau}^2} \right] \end{aligned} \tag{22-b}$$

for LSA approximation.

It is worth pointing out that due to the nano-beam deflection, the distance D presented in the Casimir force is replaced by $D - w$ and for the case of large separation gap, it is assumed that $D + R \approx D$.

3 Numerical approach for the non-linear problem

In order to numerically investigate the instability/adhesion properties and dynamic behavior of nanowires, the governing equation of motions (22-a) and (22-b) should be integrated over the time domain. In each time step of integration, the non-linear terms on the right-hand side of Eq. (22) are assumed to be a function of the values in the previous step [48]. Accurate results can then be obtained if the time steps are selected reasonably small. The reduced order model eliminates the spatial dependency in the PDEs using the Galerkin-based methods. In this method, the displacements are described as a linear combination of independent eigenmodes which must satisfy the kinematic boundary conditions. By defining the orthogonality condition of the residue to every basis function, the second-order time-dependent ODEs in terms of the generalized coordinates corresponding to the each basis function are obtained.

To find an approximate reduced-order-model (ROM), the non-dimensional deflection are assumed as $W(\xi, \tau) = \sum_{j=1}^N q_j(\tau)\phi_j(\xi)$, where N denotes the number of

considered modes, $q_j(\tau)$ denotes the time-dependent generalized coordinate of the system and $\phi_j(\xi)$ is the j th mode shape of nano-bridge which is given by

$$\phi_j(\xi) = \cosh(\lambda_j \xi) - \cos(\lambda_j \xi) - \frac{\cosh(\lambda_j) - \cos(\lambda_j)}{\sinh(\lambda_j) - \sin(\lambda_j)} (\sinh(\lambda_j \xi) - \sin(\lambda_j \xi)), \tag{23}$$

where λ_j is the root of characteristic equation for j th eigenmode. By substituting Eq. (23) into Eqs. (22-a) and (22-b), multiplying by $\phi_j(\xi)$ and integrating from $\xi = 0$ to μ_{mc} , the approximate Reduced-Order-Model on the basis of Bubnov–Galerkin decomposition method can be simplified as

$$\sum_{j=1}^N M_{ij} \ddot{q}_j(\tau) + \sum_{j=1}^N K_{ij} q_j(\tau) = F_i, \tag{24}$$

where

$$M_{ij} = (1 + \kappa_2) \int_0^1 \varphi_i \varphi_j d\xi + [\kappa_1 - \varepsilon_0(1 + \kappa_2)] \int_0^1 \varphi_i \varphi_j'' d\xi \tag{25}$$

$$K_{ij} = (1 + \mu - \sigma_1) \int_0^1 \varphi_i \varphi_j^{(iv)} d\xi - (f_i + \sigma_2) \int_0^1 \varphi_i \varphi_j'' d\xi + \varepsilon_0 f_0 \int_0^1 \varphi_i \varphi_j^{(iv)} d\xi \tag{26}$$

$$F_i = \alpha \int_0^1 \varphi_i \left(\sum_{j=1}^N \varphi_j'' q_j \right) \left(\int_0^1 \left(\sum_{j=1}^N \varphi_j' q_j \right)^2 d\xi \right) d\xi - \varepsilon_0 \alpha \int_0^1 \varphi_i \left(\sum_{j=1}^N \varphi_j^{(iv)} q_j \right) \left(\int_0^1 \left(\sum_{j=1}^N \varphi_j' q_j \right)^2 d\xi \right) d\xi$$

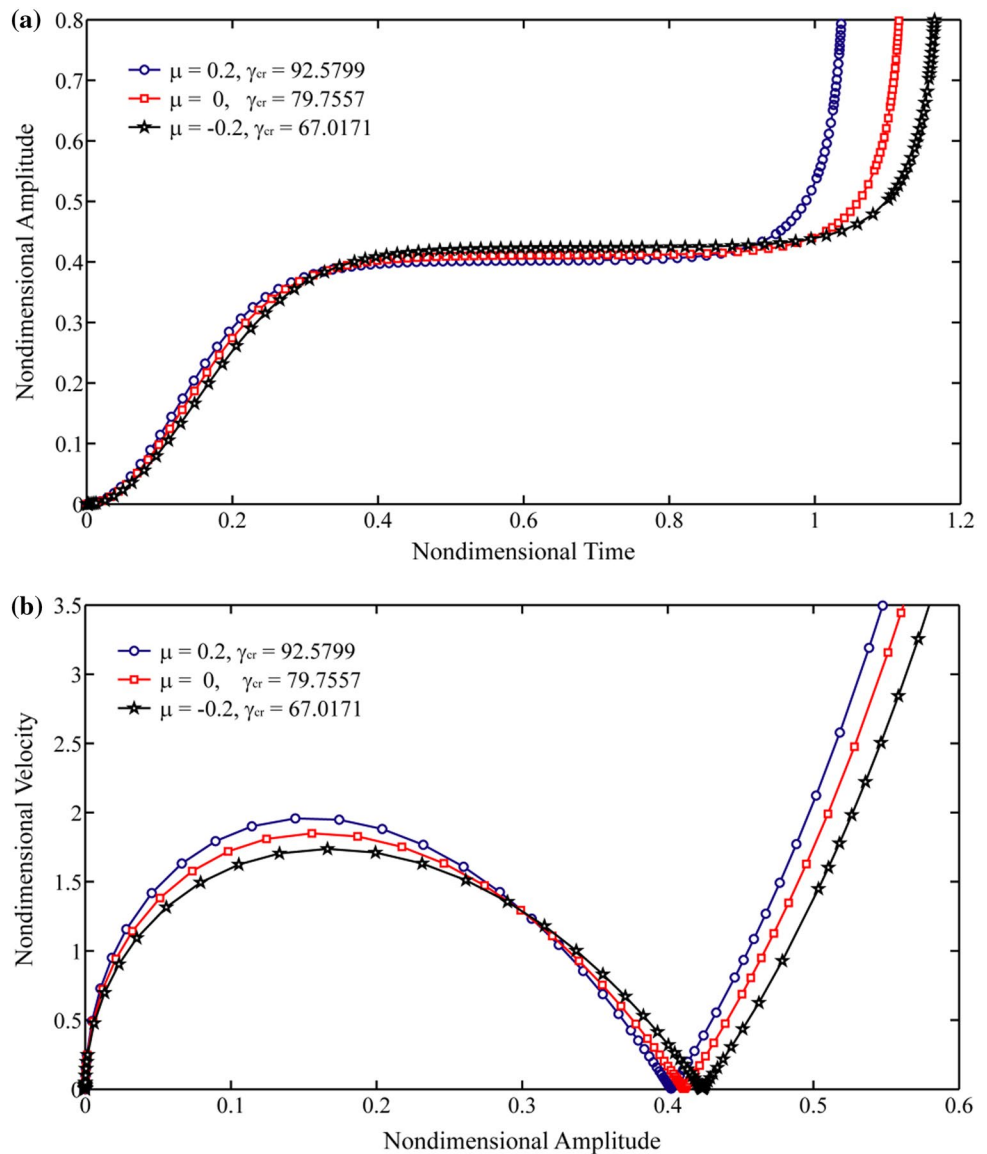
$$+ \frac{\pi^4 \gamma}{96} \int_0^1 \varphi_i \sqrt{\frac{2}{k \left(1 - \sum_{j=1}^N \varphi_j q_j \right)^7}} d\xi + \frac{49 \pi^4 \varepsilon_0 \gamma}{384} \int_0^1 \varphi_i \frac{\sqrt{2} \left(\sum_{j=1}^N \varphi_j' q_j \right)^2}{k^2 \sqrt{\left(\frac{1}{k \left(1 - \sum_{j=1}^N \varphi_j q_j \right)^7} \right)^3} \left(\left(1 - \sum_{j=1}^N \varphi_j q_j \right)^{16} \right)} d\xi$$

$$- \frac{28 \pi^4 \varepsilon_0 \gamma}{96} \int_0^1 \varphi_i \frac{\sqrt{2} \left(\sum_{j=1}^N \varphi_j' q_j \right)^2}{k \sqrt{\left(\frac{1}{k \left(1 - \sum_{j=1}^N \varphi_j q_j \right)^7} \right)^3} \left(\left(1 - \sum_{j=1}^N \varphi_j q_j \right)^9 \right)} d\xi - \frac{7 \pi^4 \varepsilon_0 \gamma}{192} \int_0^1 \varphi_i \frac{\sqrt{2} \sum_{j=1}^N \varphi_j' q_j}{k \sqrt{\left(\frac{1}{k \left(1 - \sum_{j=1}^N \varphi_j q_j \right)^7} \right)^3} \left(\left(1 - \sum_{j=1}^N \varphi_j q_j \right)^8 \right)} d\xi \tag{27-a}$$

for SSA approximation and

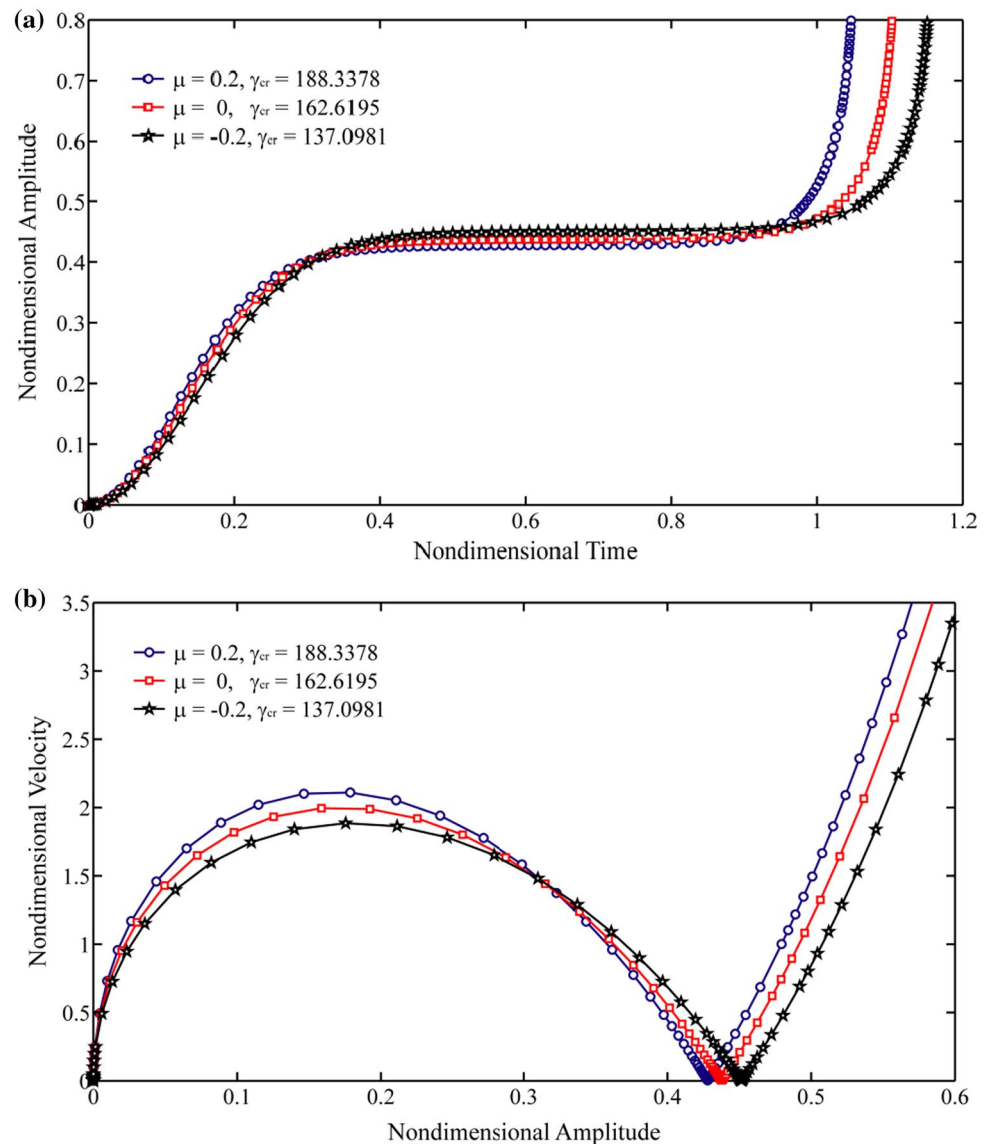
$$\begin{aligned}
 F_i = & \alpha \int_0^1 \varphi_i \left(\sum_{j=1}^N \varphi_j'' q_j \right) \left(\int_0^1 \left(\sum_{j=1}^N \varphi_j' q_j \right)^2 d\xi \right) d\xi - \varepsilon_0 \alpha \int_0^1 \varphi_i \left(\sum_{j=1}^N \varphi_j^{(iv)} q_j \right) \left(\int_0^1 \left(\sum_{j=1}^N \varphi_j' q_j \right)^2 d\xi \right) d\xi \\
 & + \gamma \int_0^1 \varphi_i \left(\frac{1}{\left(1 - \sum_{j=1}^N \varphi_j q_j\right)^3} \left[\frac{1}{\ln\left(k\left(1 - \sum_{j=1}^N \varphi_j q_j\right)\right)} + \frac{1}{2\left(\ln\left(k\left(1 - \sum_{j=1}^N \varphi_j q_j\right)\right)\right)^2} \right] \right) d\xi \\
 & - 12\varepsilon_0 \gamma \int_0^1 \varphi_i \left(\frac{\left[\frac{1}{\ln\left(k\left(1 - \sum_{j=1}^N \varphi_j q_j\right)\right)} + \frac{1}{2\left(\ln\left(k\left(1 - \sum_{j=1}^N \varphi_j q_j\right)\right)\right)^2} \right] \left(\sum_{j=1}^N \varphi_j' q_j \right)^2}{\left(1 - \sum_{j=1}^N \varphi_j q_j\right)^5} \right) d\xi \\
 & - 6\varepsilon_0 \gamma \int_0^1 \varphi_i \left(\frac{\left[\frac{1}{\ln\left(k\left(1 - \sum_{j=1}^N \varphi_j q_j\right)\right)} \right]^2 \left(1 - \sum_{j=1}^N \varphi_j q_j\right) + \frac{1}{\left(\ln\left(k\left(1 - \sum_{j=1}^N \varphi_j q_j\right)\right)\right)^3} \left(1 - \sum_{j=1}^N \varphi_j q_j\right)}{\left(1 - \sum_{j=1}^N \varphi_j q_j\right)^4} \right) \left(\sum_{j=1}^N \varphi_j' q_j \right)^2 d\xi \\
 & - 3\varepsilon_0 \gamma \int_0^1 \varphi_i \left(\frac{\left[\frac{1}{\ln\left(k\left(1 - \sum_{j=1}^N \varphi_j q_j\right)\right)} + \frac{1}{2\left(\ln\left(k\left(1 - \sum_{j=1}^N \varphi_j q_j\right)\right)\right)^2} \right] \sum_{j=1}^N \varphi_j'' q_j}{\left(1 - \sum_{j=1}^N \varphi_j q_j\right)^4} \right) d\xi \\
 & - \varepsilon_0 \gamma \int_0^1 \varphi_i \left(\frac{\left[\frac{3\left(\sum_{j=1}^N \varphi_j' q_j\right)^2}{\ln\left(k\left(1 - \sum_{j=1}^N \varphi_j q_j\right)\right)^3 \left(1 - \sum_{j=1}^N \varphi_j q_j\right)^2} + \frac{\sum_{j=1}^N \varphi_j'' q_j}{\left(\ln\left(k\left(1 - \sum_{j=1}^N \varphi_j q_j\right)\right)\right)^2 \left(1 - \sum_{j=1}^N \varphi_j q_j\right)} \right]}{\left(1 - \sum_{j=1}^N \varphi_j q_j\right)^3} \right) d\xi
 \end{aligned}$$

Fig. 8 **a** Time history and **b** phase diagram of vibrating Casimir-induced nanowire for different values of μ at corresponding adhesion time for SSA model



$$\begin{aligned}
 & -\varepsilon_0 \gamma \int_0^1 \varphi_i \left(\frac{\left[\frac{(w')^2}{\ln \left(k \left(1 - \sum_{j=1}^N \varphi_j q_j \right) \right)^2 \left(1 - \sum_{j=1}^N \varphi_j q_j \right)^2} + \frac{3 \left(\sum_{j=1}^N \varphi_j' q_j \right)^2}{\left(\ln \left(k \left(1 - \sum_{j=1}^N \varphi_j q_j \right) \right) \right)^4 \left(1 - \sum_{j=1}^N \varphi_j q_j \right)^2} \right]}{\left(1 - \sum_{j=1}^N \varphi_j q_j \right)^3} \right) d\xi \\
 & -\varepsilon_0 \gamma \int_0^1 \varphi_i \left(\frac{\left[\frac{\sum_{j=1}^N \varphi_j''' q_j}{\left(\ln \left(k \left(1 - \sum_{j=1}^N \varphi_j q_j \right) \right) \right)^3 \left(1 - \sum_{j=1}^N \varphi_j q_j \right)} \right]}{\left(1 - \sum_{j=1}^N \varphi_j q_j \right)^3} \right) d\xi \tag{27-b}
 \end{aligned}$$

Fig. 9 **a** Time history and **b** phase diagram of vibrating Casimir-induced nanowire for different values of μ at corresponding adhesion time for LSA model



for LSA approximation. In the recent equations, F_i describes the nonlinear terms. By integrating Eq. (24) over the time domain, the dynamic behavior of the system can be described.

4 Results and discussion

The Casimir force has an important role in the design and fabrication of nano-devices. To assess the influences of vacuum fluctuations on the dynamics and instability characteristics of nano-systems, the variations of non-dimensional gap ($1 - W$) versus the Casimir parameter are drawn for SSA and LSA models. Figure 4 shows the non-dimensional gap as a function of Casimir force parameter γ for some values of geometry parameter k . Any increase in the Casimir

parameter can decrease the initial gap between the flexible nanowire and bottom plate. According to the illustrated results, it is inferred that any increase in the Casimir parameter leads to increase in the dynamic deflection of nano-beam. In addition, when the Casimir parameter approaches to the critical value γ_{cr} , the nano-beam loses its stability and adheres to the fixed substrate. On the other hand, one can clearly observe that for both SSA and LSA approximations, the significant effect of geometry parameter k is to increase γ_{cr} . In addition, it is shown that the effect of parameter k in the case of small separations is more significant than large separations. Finally, one can see that for small separation gaps the nanowire may collapse into contact with the bottom plate at lower values of Casimir parameter in comparison with large separation gaps. It should be noted that if the nanowire length is greater

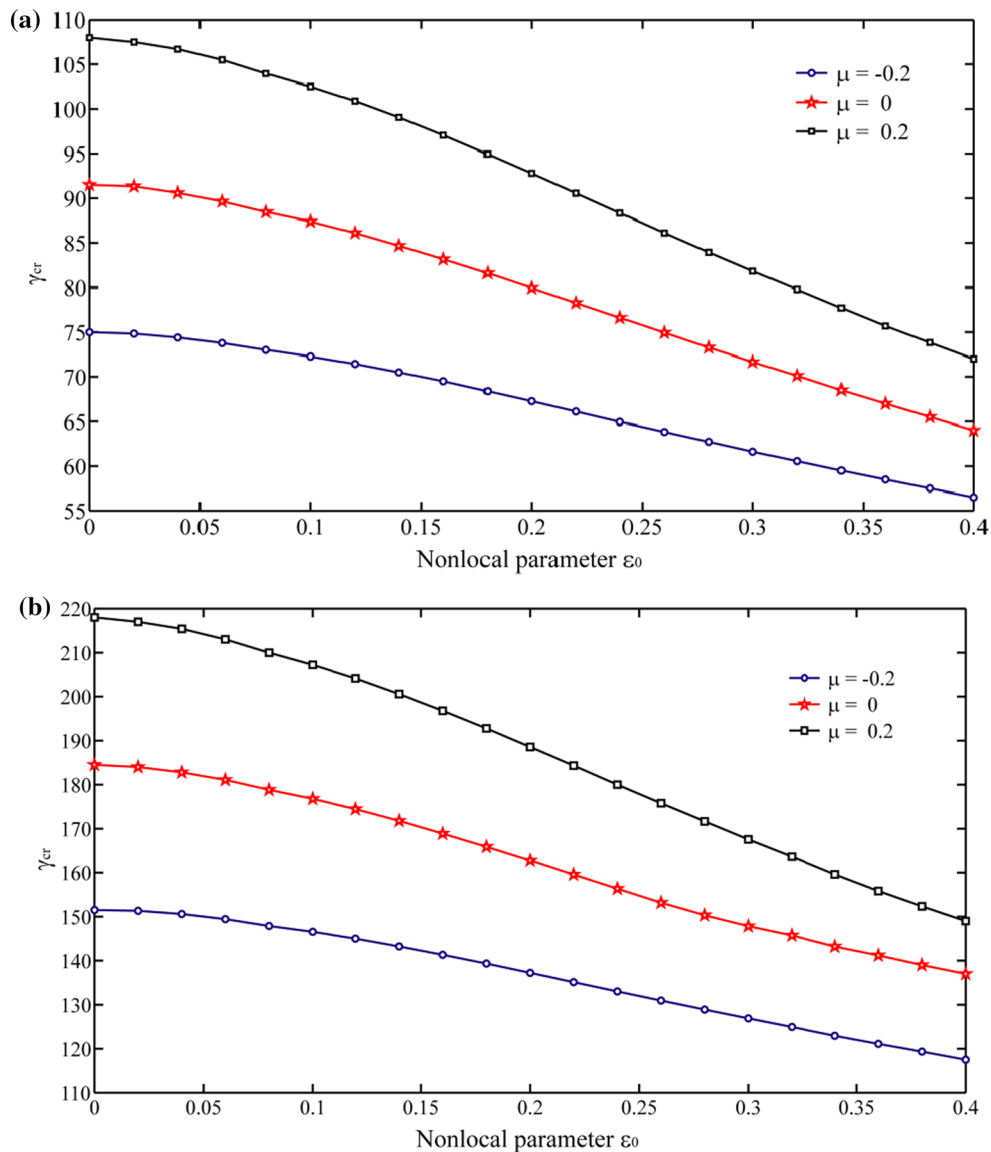


Fig. 10 The relation between γ_{cr} and nonlocal parameter ϵ_0 ; investigating the effect of surface parameter μ for **a** SSA and **b** LSA models

than the critical length (i.e. detachment length) any disturbance in the fabrication process can result in the instability of the structure even in the absence of any actuation voltages.

Figure 5a, b shows the non-dimensional gap $(1 - W)$ versus the Casimir parameter γ for different values of the nonlocal parameter ϵ_0 considering the SSA and LSA models, respectively. It is observed that by increasing the nonlocal parameter, the mid-point of the nano-bridge diverges to the bottom substrate at lower values of Casimir parameter ϵ_0 which means that the dynamic instability of nano-structure happens at lower values of nanowire length as the size-effect parameter ϵ_0 increases.

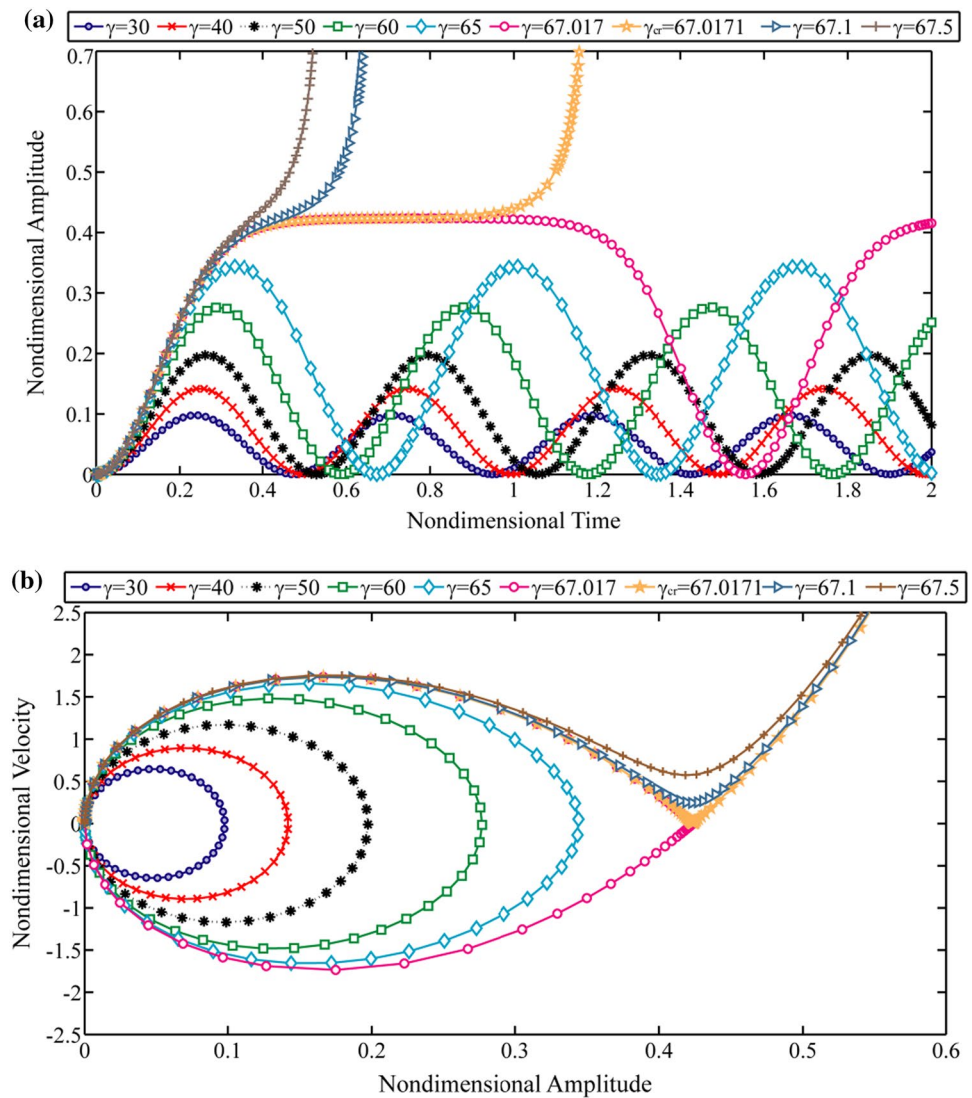
The influence of the non-dimensional parameter μ , i.e. the effect of the surface elasticity in the dynamic instability

of nonlocal nanowires, is shown in Fig. 6a, b. It is seen that the predicted critical values for Casimir parameter increases as the parameter μ increases, for both SSA and LSA models.

The time responses of vibrating nanowires for various values of geometry parameter k at the corresponding adhesion time are illustrated in Fig. 7. According to this figure, for both SSA and LSA approaches, the adhesion time of the nano-beam is increased by increasing the geometry parameter and the dynamic instability occurs at higher values of Casimir force parameter γ .

Figures 8 and 9 illustrate the time histories and phase portraits of Casimir-induced nanowires at the corresponding adhesion times for some given values of non-dimensional surface parameter μ . According to the obtained results, it is

Fig. 11 Effect of Casimir parameter on the instability characteristics of nanowires for SSA model, **a** time history **b** phase portrait



clearly inferred that for both small and large separation gaps, by increasing the parameter μ , the adhesion time decreases. Moreover, by increasing the parameter μ , the dynamic instability occurs at higher values of Casimir force. In addition, one can see that as the surface effect parameter μ increases, the corresponding deflection slightly decreases and instability happens at lower values of nano-beam deflection.

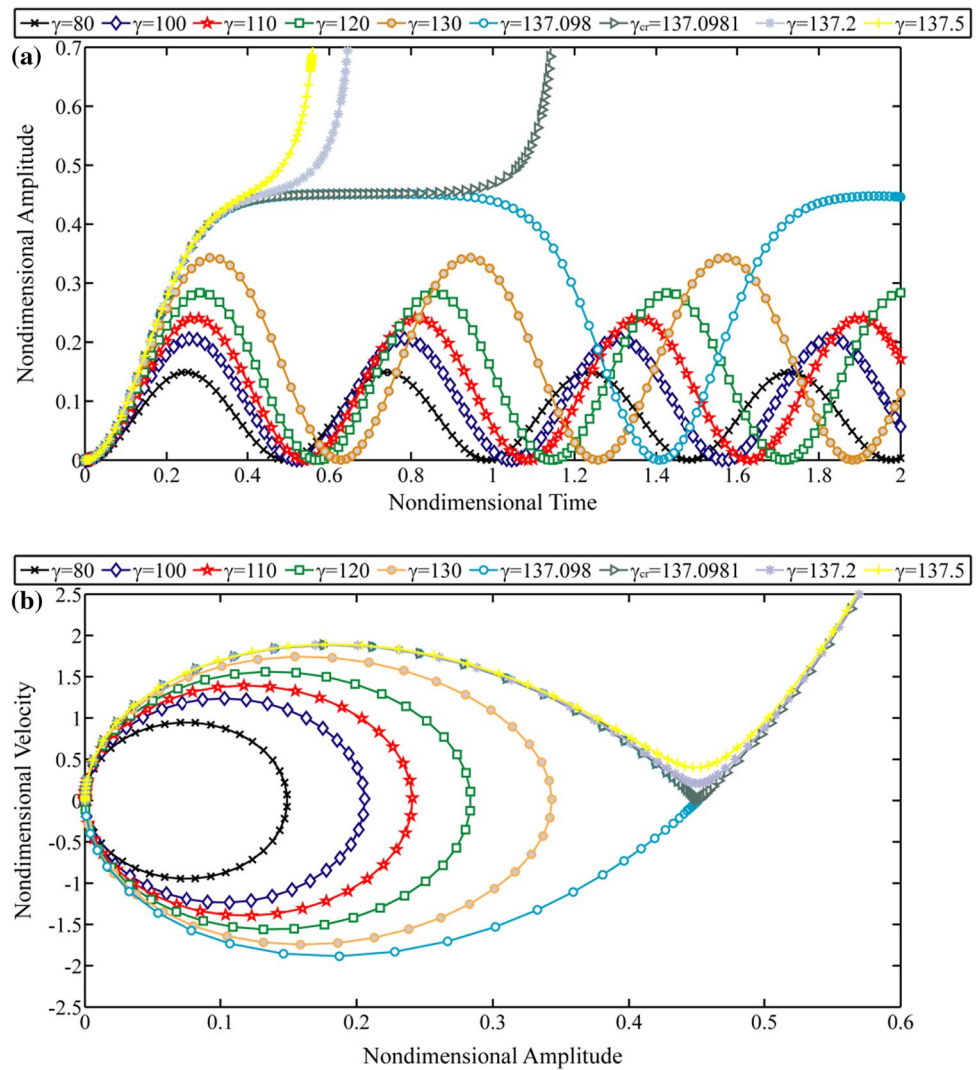
The effect of the nonlocal parameter ε_0 which accounts for the size dependency of nanowire on the critical values of Casimir force is illustrated in Fig. 10a, b. The obtained results elucidate that γ_{cr} decreases by increasing the nonlocal parameter. Furthermore, it is concluded from this figure that the positive μ , which stands for the surface elasticity, can increase the critical Casimir value of nanowires while the negative one will decrease it.

The plot of time responses and phase portraits of the Casimir-induced nanowires may be of interest. To this end, the influence of Casimir force on the instability characteristics of nanowires is investigated through Figs. 11 and 12 for

the case of SSA and LSA models, respectively. According to illustrated results in Figs. 11a and 12a, one can observe that the nano-beam deflection and time period of vibrating nanowires under the influence of Casimir force is increased by increasing parameter γ up to the adhesion time. On the other hand, in the vicinity of adhesion state, any increase in the Casimir parameter changes the dynamic behavior of the system and causes the nanowire to drop to the fixed plate.

It is observed from Figs. 11b and 12b that at lower values of Casimir parameter, the system exhibits the periodic motions around the stable center point. When the dynamic instability occurs at critical Casimir value ($\gamma_{cr} = 67.0171$ for SSA and $\gamma_{cr} = 137.0981$ for LSA models), a homoclinic orbit appears in the phase plane which separates periodic solutions from the unbounded non-periodic trajectories around an unstable saddle node. The homoclinic orbit starts from the unstable branch of saddle node and returns to it via the stable one. In addition, one can conclude that

Fig. 12 Effect of Casimir parameter on the instability characteristics of nanowires for LSA model, **a** time history **b** phase portrait



the Casimir-induced nanowire collapses to the bottom plate beyond the unstable saddle node.

5 Conclusions

In this research work, the significant effects of Casimir force, nonlocal and surface effects on instability/adhesion properties of suspended nanowires were investigated. For this purpose, considering both small and large separation regimes, the non-linear governing equation of vibrating nanowires was extracted and solved using a step-by-step numerical approach. Based on the results, the effect of geometry parameter k was to increase the critical Casimir value of nanowires for both SSA and LSA models. It was also observed that the critical Casimir value decreases as the nonlocal parameter increases. In addition, the effect of surface elasticity

parameter was to increase the critical Casimir value and to decrease the adhesion time. Finally, it was found that at lower values of Casimir force, the nanowire showed periodic motions around the stable center point. By increasing the Casimir force, the nano-system experiences unbounded non-periodic motions in the vicinity of unstable saddle node.

References

1. Wang ZL (2004) Mechanical properties of nanowires and nanobelts. *Dekker Encycl Nanosci Nanotechnol* 2:1773–1786
2. Craighead HG (2000) Nanoelectromechanical systems. *Science* 290:1532–1535
3. Wang MCP, Gates BD (2009) Directed assembly of nanowires. *Mater Today* 12:34–43
4. Khajeansari A, Baradaran GH, Yvonnet J (2012) An explicit solution for bending of nanowires lying on Winkler–Pasternak

- elastic substrate medium based on the Euler–Bernoulli beam theory. *Int J Eng Sci* 52:115–128
5. Serre P, Ternon C, Stambouli V, Perival P, Baron T (2013) Fabrication of silicon nanowire networks for biological sensing. *Sens Actuators B* 182:390–395
 6. Patolsky F, Zheng G, Lieber CM (2006) Nanowire-based biosensors. *Anal Chem* 78(13):4260–4269
 7. Husain A, Hone J, Postma HWC, Huang XMH, Drake T, Barbic M, Scherer A, Roukes ML (2003) Nanowire-based very-high-frequency electromechanical resonator. *Appl Phys Lett* 83:1240
 8. Feng XL, He R, Yang P, Roukes ML (2007) Very high frequency silicon nanowire electromechanical resonators. *Nano Lett* 7(7):1953–1959
 9. Farrokhabadi A, Abadian N, Rach R, Abadyan M (2014) Theoretical modelling of the Casimir force-induced instability in freestanding nanowires with circular cross-section. *Phys E* 63:67–80
 10. Zou J, Marcet Z, Rodriguez AW, Reid MTH, McCauley AP, Kravchenko II, Lu T, Bao Y, Johnson SG, Chan HB (2013) Casimir forces on a silicon micromechanical chip. *Nat Commun* 4:1845
 11. Lombardo FC, Mazzitelli FD, Villar PI (2008) Numerical evaluation of the Casimir interaction between cylinders. *Phys Rev D* 78:085009
 12. Emig T, Jaffe RL, Kardar M, Scardicchio A (2006) Casimir interaction between a plate and a cylinder. *Phys Rev Lett* 96:080403
 13. Terças H, Ribeiro S, Mendonça JT (2015) Quasi-polaritons in Bose-Einstein condensates induced by Casimir–Polder interaction with graphene. *J Phys Condens Matter* 27:214011
 14. Ali S, Terças H, Mendonça JT (2011) Nonlocal plasmon excitation in metallic nanostructures. *Phys Rev B* 83:153401
 15. Bordag M, Mohideen U, Mostepanenko VM (2001) New developments in the Casimir effect. *Phys Rep* 353:1–205
 16. Casimir HBG (1948) On the attraction between two perfectly conducting plates. *Proc K Ned Akad Wet* 51:793
 17. Guo JG, Zhao YP (2004) Influence of van der Waals and Casimir Forces on Electrostatic Torsional Actuators. *J Microelectromech Syst* 13(6):1027
 18. Lin WH, Zhao YP (2005) Nonlinear behavior for nanoscales electrostatic actuators with Casimir force. *Chaos Solitons Fractals* 23:1777
 19. Casimir HBG, Polder D (1948) The influence of retardation of the London-van der Waals forces. *Phys Rev* 73:360
 20. Teo LP (2011) First analytic correction to the proximity force approximation in the Casimir effect between two parallel cylinders. *Phys Rev D* 84:065027
 21. Teo LP (2011) Casimir, interaction between a cylinder and a plate at finite temperature: exact results and comparison to proximity force approximation. *Phys Rev D* 84:025022
 22. Barretta R, Feo L, Luciano R, Marotti de Sciarra F (2015) Variational formulations for functionally graded nonlocal Bernoulli–Euler nanobeams. *Compos Struct* 129:80–89
 23. Sedighi HM, Daneshmand F, Abadyan M (2015) Modified model for instability analysis of symmetric FGM double-sided nano-bridge: corrections due to surface layer, finite conductivity and size effect. *Compos Struct* 132:545–557
 24. Sedighi HM (2014) The influence of small scale on the Pull-in behavior of nonlocal nano-Bridges considering surface effect, Casimir and van der Waals attractions. *Int J Appl Mech*. doi:10.1142/S1758825114500306
 25. Koochi A, Kazemi A, Khandani F, Abadyan M (2012) Influence of surface effects on size-dependent instability of nano-actuators in the presence of quantum vacuum fluctuations. *Phys Scr* 85(3):035804
 26. Abdi J, Koochi A, Kazemi AS, Abadyan M (2011) Modeling the effects of size dependence and dispersion forces on the pull-in instability of electrostatic cantilever NEMS using modified couple stress theory. *Smart Mater Struct* 20:055011
 27. Karimipour I, Tadi Beni Y, Koochi A, Abadyan M (2015) Using couple stress theory for modeling the size-dependent instability of double-sided beam-type nanoactuators in the presence of Casimir force. *J Braz Soc Mech Sci Eng*. doi:10.1007/s40430-015-0385-6
 28. AkbarzadehKhorshidi M, Shariati M (2015) Free vibration analysis of sigmoid functionally graded nanobeams based on a modified couple stress theory with general shear deformation theory. *J Braz Soc Mech Sci Eng*. doi:10.1007/s40430-015-0388-3
 29. Sedighi HM (2014) Size-dependent dynamic pull-in instability of vibrating electrically actuated micro-beams based on the strain gradient elasticity theory. *Acta Astronaut* 95:111–123
 30. Shojaeian M, Tadi Beni Y, Ataei H (2016) Electromechanical buckling of functionally graded electrostatic nanobridges using strain gradient theory. *Acta Astronaut* 118:62–71
 31. Ansari R, Gholami R, Sahmani S (2013) Size-dependent vibration of functionally graded curved microbeams based on the modified strain gradient elasticity theory. *Arch Appl Mech* 83(10):1439–1449
 32. Daneshmand F (2014) Combined strain-inertia gradient elasticity in free vibration shell analysis of single walled carbon nanotubes using shell theory. *Appl Math Comput* 243:856–869
 33. Wang ZQ, Zhao YP, Huang ZP (2010) The effects of surface tension on the elastic properties of nano structures. *Int J Eng Sci* 48:140–150
 34. Dingrevillea R, Qua J, Cherkaoui M (2005) Surface free energy and its effect on the elastic behavior of nano-sized particles, wires and films. *J Mech Phys Solids* 53(8):1827–1854
 35. Gurtin ME, Murdoch AI (1978) Surface stress in solids. *Int J Solids Struct* 14:431–440
 36. Sedighi HM (2015) Modeling of surface stress effects on the dynamic behavior of actuated non-classical nano-bridges. *Trans Can Soc Mech Eng* 39(2):137–151
 37. Eltaher MA, Mahmoud FF, Assie AE, Meletis EI (2013) Coupling effects of nonlocal and surface energy on vibration analysis of nanobeams. *Appl Math Comput* 224:760–774
 38. Fu Y, Zhang J (2011) Size-dependent pull-in phenomena in electrically actuated nanobeams incorporating surface energies. *Appl Math Model* 35(2):941–951
 39. Koochi A, Hosseini-Toudeshky H, Ovesy HR, Abadyan M (2013) Modeling the influence of surface effect on instability of nano-cantilever in presence of Van der Waals force. *Int J Struct Stab Dyn* 13:1250072
 40. Zhang WM, Yan H, Peng ZK, Meng G (2014) Electrostatic pull-in instability in MEMS/NEMS: a review. *Sens Actuators A* 214:187–218
 41. Bordag M, Mohideen U, Mostepanenko VM (2001) New developments in the Casimir effect. *Phys Rep* 353:1
 42. Lamoreaux SK (2005) The Casimir force: background, experiments, and applications. *Rep Prog Phys* 68:201–236
 43. Chan HB, Bao Y, Zou J, Cirelli RA, Klemens F, Mansfield WM, Pai CS (2008) Measurements of the Casimir force between a gold sphere and a silicon surface with nanoscale v trench arrays. *Phys Rev Lett* 101:030401
 44. Li H, Kardar M (1991) Fluctuation-induced forces between rough surfaces. *Phys Rev Lett* 67:3275
 45. Buscher R, Emig T (2005) Geometry and spectrum of Casimir forces. *Phys Rev Lett* 94:133901
 46. Rahi SJ, Emig T, Jaffe RL, Kardar M (2008) Casimir forces between cylinders and plates. *Phys Rev A* 78:012104
 47. Bulgac A, Magierski P, Wirzba A (2006) Scalar Casimir effect between Dirichlet spheres or a plate and a sphere. *Phys Rev D* 73:025007
 48. Abbasnejad B, Rezaazadeh G, Shabani R (2013) Stability analysis of a capacitive fgm micro-beam using modified couple stress theory. *Acta Mech Solida Sin* 26(4):427–440